Electrocatalysis of Peroxide Reduction by Au-Stabilized, Fe-Containing Poly(vinylpyridine) Films

Jongwon Kim and Andrew A. Gewirth*

Department of Chemistry and Frederick Seitz Materials Research Laboratory, University of Illinois at Urbana−Champaign, Urbana, Illinois 61801

Received: February 7, 2005; In Final Form: March 19, 2005

We show that poly(vinylpyridine) (PVP) coated glassy carbon surfaces containing $Fe(CN)_6^{3-}$ exhibit catalytic activity toward electroreduction of H_2O_2. While $Fe(CN)_6^{3-}$ is catalytically inactive in solution phase, it exhibits catalytic activity upon incorporation into the PVP film, because film incorporation leads to an open coordination site in the otherwise inert $Fe(CN)_6^{3-}$ molecule. However, this catalytic activity is quickly lost during H_2O_2 electroreduction due to leaching of the Fe species from the PVP film. The Fe catalyst in the PVP film could be stabilized by 1 order of magnitude in time by electrodeposition of small Au particles. Characterization of the film using scanning electron microscopy, secondary ion mass spectroscopy, and Raman spectroscopy shows that covalent attachment between the Au particle and the Fe-based catalyst is a likely mechanism for catalyst stabilization.

1. Introduction

Electroreduction of dioxygen is one of the most important reactions in electrochemistry because of the central role it plays in fuel cell, corrosion, and industrial processes. The electrocatalytic reduction of dioxygen and hydrogen peroxide, the main intermediate of dioxygen reduction, has been extensively studied.[1,2] A major focus at present is replacing the precious metal based catalysts currently used with those utilizing cheaper metals and additionally featuring lower activation overpotentials. Several different approaches have been examined over the course of the past 40 years to circumvent Pt in low-temperature cathodes. These include (1) modification of the Pt material by alloying,[3] (2) modification of Pt or related precious metals by decoration of nanoparticles,[4,5] (3) use of bioinspired catalysts,[6−8] (4) use of combinatorial approaches,[9] and (5) use of first-row transition metal based catalyst supported on C.[10]

Among the studies related to the metal complex systems, complexes incorporating Fe exhibit unique catalytic activity toward H_2O_2 electroreduction. Anson and co-workers showed that iron porphyrins adsorbed on electrode surfaces provide catalytic pathways for electroreduction of dioxygen and hydrogen peroxide.[11,12] Other Fe complexes such as Fe-coordinated alizarin complexone,[13] Fe−adenosine phosphate,[14] and Fe-substituted silicotungstate[15] also show catalytic activity for electroreduction of H_2O_2. Misono and co-workers showed that Fe-substituted silicotungstates utilize H_2O_2 catalytically for organic compound epoxidation reactions. They showed that iron works better than other transition metals such as Cu and Mn as a substituted metal atom for the catalytic reaction.[16,17]

One central challenge in using molecular species as catalysts for processes such as peroxide and dioxygen electroreduction is stabilizing the catalyst on the electrode surface. This challenge is especially acute for oxygen reduction, since catalytic activity in acid solution at very positive potentials is desired. These positive potentials typically lead to leaching of the active metal and attenuation of catalyst response.

One way to attach catalysts to electrode surfaces is by utilizing electrode surfaces modified with polymer matrixes. Electrode modification based on polymer matrixes has been extensively investigated for its utilization in electrocatalysis. Among the polymers employed for this application, poly(vinylpyridine) (PVP) has been shown to be an effective matrix for the incorporation of anionic species that have electrochemical activities. Anson and co-workers extensively studied the electrochemical behaviors of metal complexes attached to electrode surfaces coated with PVP.[18−25] Ru−EDTA complexes can be coordinatively attached to the PVP films, which were found to catalyze the electron transfer of Fe^{III}/Fe^{II} couple.[18−20,22] Other metal complexes such as $Fe(CN)_6^{3-}$ and $IrCl_6^{2-}$ have been shown to be incorporated to the films through the electrostatic interaction between negatively charged metal complexes and protonated PVP films.[20,21,24]

In addition to acting as supports for these molecular catalysts, polymer coated electrode surfaces have also been modified by deposition of metal particles for catalytic applications. Pt particles deposited on a poly(vinylacetic acid) coated glassy carbon electrode (GCE) exhibit high catalytic activities for both the hydrogen evolution reaction and oxygen reduction.[26] Bartak and co-workers utilized PVP-coated GCE as substrates for metal deposition and showed that metal microparticles such as Pt, Pd, Ir, and Ru exhibit catalytic activities with regard to hydrogen evolution from acidic solutions.[27,28] In these studies, they achieved a large surface area with low loading levels, high catalytic efficiency, and excellent stability. Scanning electron microscopy (SEM) images revealed that these metal microparticles nucleated at the electrode surface and grew through the polymers at the sites of nucleation.[27] Other polymers such as poly(phenylenediamine), polyanaline, and poly(ethylenedioxythiophene) have also been employed as matrixes for Pt particle deposition, and their electrocatalytic activities toward oxygen and hydrogen peroxide have been reported.[29−31]

In this paper, we investigate the electrocatalytic activity of iron-containing PVP films toward H_2O_2 reduction. $Fe(CN)_6^{3-}$ species confined on the PVP coated electrode surface exhibit

* To whom correspondence should be addressed. Telephone: (217) 333-8329; Fax: (217) 333-2685. E-mail: agewirth@uiuc.edu.

10.1021/jp050672h CCC: $30.25
Published on Web 04/16/2005

catalytic activity, and further deposition of Au on this film enhanced and stabilized the catalytic activity. Detailed characterization of the film was conducted by scanning electron microscopy (SEM), secondary ion mass spectroscopy (SIMS), and Raman spectroscopy.

2. Experimental Section

All solutions were prepared using purified water (Milli-Q UV plus, 18.2 MΩ cm). The supporting electrolyte was acetate buffer, prepared by partial neutralization of 0.1 M CH_3COOH (99.9985%, Alfa Aesar) to pH 4.7 with NaOH. $K_3Fe(CN)_6$ (Fisher), PVP (Aldrich, average MW = 60 000), and $KAuCl_4$ (Aldrich) were used as received.

PVP films were spin-coated on GCE from stock solutions of the polymer in 2-propanol (0.50 wt %) and dried in air for 10 min. $Fe(CN)_6^{3-}$ was incorporated in PVP film by dipping the film into a solution containing 5 mM $K_3Fe(CN)_6$ + 0.1 M acetate buffer for 5 min. For Au deposition, the modified electrode was put into a solution containing 1 mM $KAuCl_4$ + 0.1 M acetate buffer and the potential was either cycled between 0.8 and −0.2 V at a scan rate of 50 mV/s or stepped from +0.8 to −0.2 V and holding at this potential for 60 s.

Electrochemical measurements were conducted using a CHI 620A potentiostat (CH Instrument, Austin, TX) and the solution was purged with Ar prior to use. A commercially available GCE with diameter = 0.3 cm (Bioanalytical Systems, West Lafayette, IN) was employed as the working electrode. Au wire and Ag/AgCl electrodes were used as counter and reference electrodes, respectively. All potentials are reported relative to the Ag/AgCl reference electrode (+0.20 V vs the normal hydrogen electrode). For kinetic measurements, the working electrode was rotated using a Pine Model MSRX rotator.

SEM characterization of the films was performed using a Hitachi S-4700 Cold FE-SEM (Hitachi High Technologies, Pleasanton, CA) with an acceleration voltage of 10 kV. Image analysis was accomplished using Scion Image for Windows (Scion Corporation, MD) and WSxM software (Nanotec, Spain). Time-of-flight secondary ion mass spectrometry (ToF SIMS) was performed using a PHI Trift III ToF SIMS (Physical Electronics, Chanhassen, MN). An Au^+ ion beam with a current density of 0.026 mA/cm^2 was used as the primary ion source. A 400 × 400 μm^2 area was sputtered by the O_2^+ beam for 5 s, and secondary ions from the central 50 × 50 μm^2 of the resulting crater were analyzed for 7 s and monitored as a function of sputtering time. Raman spectroscopy was performed using an Innova-90 Ar ion laser (Coherent) which provided Raman excitation at 514.5, 488, and 458 nm. The scattered radiation was collected with a camera lens (85 mm, Canon) and focused at the entrance slit of a three-stage monochromator (1877 Triplemate, Spex). The spectral resolution was estimated to be 3 cm^{-1}.

3. Results

3.1. Electrochemical Properties of Fe/PVP/GCE. *3.1.1. Properties without Addition of H_2O_2.* Figure 1A shows cyclic voltammograms obtained from a bare GCE in 1 mM $Fe(CN)_6^{3-}$ + 0.1 M acetate buffer in the presence and absence of H_2O_2. The dashed line in Figure 1A was obtained absent H_2O_2 and shows a reversible redox wave with a midpoint potential E_{mid} = 0.19 V. Here, $E_{mid} = (E_a + E_c)/2$ and E_a and E_c are the anodic and cathodic peak potentials, respectively. The addition of 10 mM of H_2O_2 to the 1 mM $Fe(CN)_6^{3-}$ + 0.1 M acetate buffer solution does not change the electrochemical response of GCE as shown by the solid line in Figure 1A. This means that

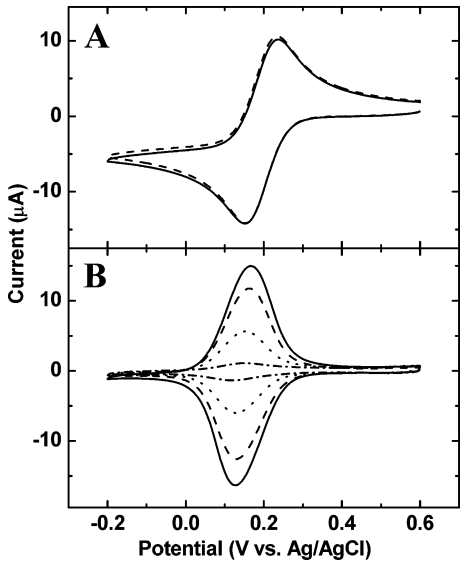

Figure 1. (A) Cyclic voltammograms obtained from a bare GCE in 1 mM $K_3Fe(CN)_6$ + 0.1 M acetate buffer in the absence (dashed line) and presence of 10 mM H_2O_2 (solid line). (B) Time dependence of cyclic voltammograms of PVP films containing $Fe(CN)_6^{3-}$ on a GCE in 0.1 M acetate buffer. Solid, dashed, and dotted lines were obtained 0, 10, and 60 min, respectively, after dipping the electrode into the solution. The dash−dot line was obtained after 10 min of rotating the electrode (1000 rpm) followed by the dotted line. The scan rate was 50 mV/s.

$Fe(CN)_6^{3-}$ species in solution do not catalyze H_2O_2 reduction on the GCE surface.

We speculated that confining the Fe species to the electrode surface would allow this species to participate in catalysis. Indeed, there is considerable precedent to suggest that surface-confined metal species exhibit significant additional activity relative to the solution phase.[11,32] Figure 1B shows the electrochemical response obtained from the $Fe(CN)_6^{3-}$ species confined on the electrode surface through the electrostatic interaction with protonated PVP films in 0.1 M acetate buffer solution. The effective pK_a of protonated pyridine groups in PVP has been estimated to be ca. 5.3.[24] The redox wave from this (Fe/PVP/GCE) system exhibits E_{mid} = 0.15 V and a peak separation of 40 mV. The reduced peak separation compared with that of 81 mV obtained on a bare GCE in $Fe(CN)_6^{3-}$ solution indicates the redox couples are confined on the electrode surface.[33] By integrating the current, we determine that the total quantity of $Fe(CN)_6^{3-}$ incorporated in the PVP film is ca. 8.0 (±0.9) × 10^{-9} mol/cm^2.

Figure 1B also shows the effect of time on the Fe/PVP/GCE voltammetry. The figure shows that the current is relatively large initially, but then the response decays quickly, so that at 60 min only ca. 40% of the $Fe(CN)_6^{3-}$ remains in the film. The peak separation for the Fe/PVP/GCE system changes from 40 mV initially to 33 mV after 10 min and 25 mV after 60 min. Additionally, the dash−dot trace in Figure 1B shows the result of rotating the electrode in pure electrolyte for 10 min after prior holding for 60 min. At this point the current decreases to a level some 20% below that observed at 60 min. This shows that rotating the sample can help to remove the Fe material from the PVP. The origin of this leaching behavior will be discussed below. Unfortunately, we were not able to obtain the scan rate dependence of the voltammetry due to the lability of the Fe species from the polymer matrix.

There are two previous papers examining the incorporation of anionic metal species into quaternized PVP (QPVP). In the

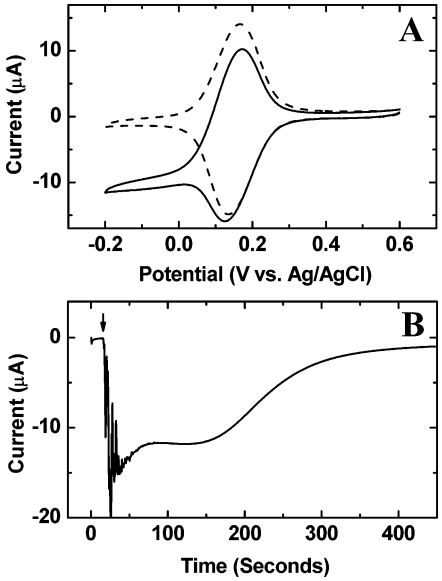

Figure 2. (A) Cyclic voltammograms of PVP films containing $Fe(CN)_6^{3-}$ on a GCE in 0.1 M acetate buffer in the absence (dashed line) and presence of 10 mM H_2O_2 (solid line). The scan rate was 50 mV/s. (B) Time dependence of the cathodic current obtained at 0.1 V on Fe/PVP/GCE rotated at 500 rpm in 0.1 M acetate buffer solution. 10 mM H_2O_2 was injected at time = 25 s (denoted by arrow).

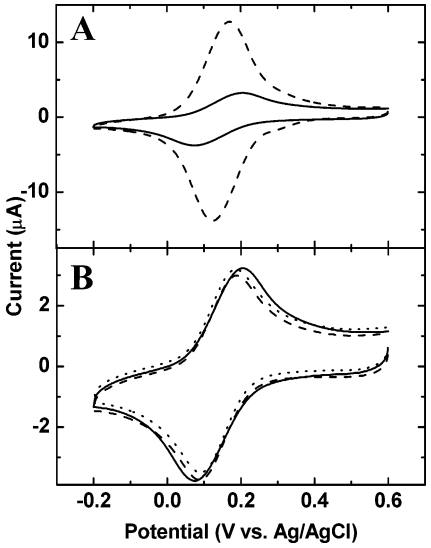

Figure 3. (A) Cyclic voltammograms of $Fe(CN)_6^{3-}$ containing PVP films on GCE before (dashed line) and after (solid line) Au deposition in 0.1 M acetate buffer solution. (B) Time dependence of cyclic voltammograms of Au/Fe/PVP/GCE in 0.1 M acetate buffer. Solid and dashed lines were obtained 0 and 30 min, respectively, after dipping the electrode into the solution. The dotted line (offset by 0.2 μA for clarity) was obtained after rotating the electrode (1000 rpm) for 10 min followed by the dashed line. Scan rate was 50 mV/s.

first,[24] $Fe(CN)_6^{3-}$ was incorporated into a quaternized PVP film with a surface coverage of ca. $\Gamma(Fe(CN)_6^{3-}) = 3.5 \times 10^{-9}$ mol/cm^2 (pH 1), a quantity which was interpreted to suggest that most of the N^+ sites were associated with the Fe complex. No information regarding the stability of the Fe complex with potential sweep or immersion time was provided in this paper. In the second,[34] $IrCl_6^{3-}$ was associated with quaternized PVP (QPVP) with $\Gamma(IrCl_6^{3-}) = (0.67-1.74) \times 10^{-8}$ mol/cm^2, a number interpreted to suggest that between 10 and 30% of the N^+ sites were associated with the Ir complex. In this case, $IrCl_6^{3-}$ was found to be stable in QPVP under stationary conditions. A slight loss of $IrCl_6^{3-}$ from the polymer was found immediately after immerson in pure electrolyte solution, but after 10−15 min, 85−90% remained. Subsequent losses were very small under stationary conditions (180 min). However, severe losses occurred when the electrode was rotated (450 rpm): 64% remained after 80 min of rotation. Unfortunately, we found that the $IrCl_6^{3-}$-incorporated QPVP film exhibited no activity for peroxide reduction, a feature that made it unsuitable for this project.

We examined the relative stability of $Fe(CN)_6^{3-}$ in protonated PVP vs QPVP in acetate buffer without addition of peroxide. $Fe(CN)_6^{3-}$ leaches out of QPVP more slowly than from protonated PVP; after 90 min ca. 50% remains in QPVP while 33% remains in protonated PVP. However, as we show below, $Fe(CN)_6^{3-}$ incorporated in protonated PVP quickly loses catalytic activity toward peroxide reduction, a feature that it shares with the QPVP material (for QPVP the catalytic current drops down to ca. 20% of its initial value after 15 potential cycles between 0.6 and −0.2 V in the presence of H_2O_2). Since we could incorporate somewhat more Fe complex in the protonated PVP relative to the QPVP film, we elected to use this more easily prepared material in subsequent investigations.

3.1.2. Addition of H_2O_2 to the Fe/PVP/GCE System. The solid line in Figure 2A shows the effect of addition of 10 mM H_2O_2 to the solution. The voltammogram features an enhanced cathodic current commencing at ca. 0.15 V, which corresponds to the cathodic peak potential of the $Fe^{III}(CN)_6^{3-}/Fe^{II}(CN)_6^{4-}$ couple. For both the bare GCE and the PVP-modified GCE, current associated with peroxide reduction is not observed until ca. −0.7 V. This suggests that the $Fe(CN)_6^{3-}$ species confined on the electrode surface exhibits electrocatalytic activity for H_2O_2 reduction.

Figure 2B shows the time dependence of the cathodic current with the potential held at 0.1 V for the Fe/PVP/GCE system rotating at 500 rpm obtained in 10 mM H_2O_2 + 0.1 M acetate buffer solution. The graph shows that the magnitude of the current increases for the first 10 s following H_2O_2 injection as mixing within the cell occurs and then decreases and levels off to a plateau until a time of about 150 s after injection. At this point the current decreases exponentially with a time constant of 1.0×10^{-2} s^{-1}, and after 400 s, the cathodic current is less than 1 μA. At the long times considered here, the cathodic current must be associated with peroxide reduction. The drop in current shows that the electrode is becoming deactivated. We showed above that, even without rotation, Fe leaches from the polymer and this leaching is likely the origin of the deactivation of the electrode, which is faster with rotation, as found previously.[34]

3.2. Effect of Au Particle Addition to the Fe/PVP/GCE System. We examined different schemes to impart stability to the Fe/PVP/GCE system. Interestingly, we found that deposition of Au onto the film from a $KAuCl_4$ solution imparts nearly an order of magnitude more stability to the system. Figure 3A shows the voltammetry obtained from the Fe/PVP/GCE system in a solution containing only acetate buffer (pH 4.7) compared with that from the Au-deposited Fe/PVP/GCE (Au/Fe/PVP/GCE) in the same solution. After Au deposition, the peak height of the current associated with the $Fe^{III}(CN)_6^{3-}/Fe^{II}(CN)_6^{4-}$ couple decreases to 30% of its initial value while the peak separation increases to 135 mV. The decrease of current from the $Fe^{III}(CN)_6^{3-}/Fe^{II}(CN)_6^{4-}$ couple upon Au decoration can be attributed to reduced access of electroactive sites to solution. The large peak separation values (>ca. 60 mV) are indicative of slow electron transfer between the electrode surface and the redox centers in the polymer films.[35] In this case, the increase in peak separation implies that diffusion of $Fe(CN)_6^{3-}$ species

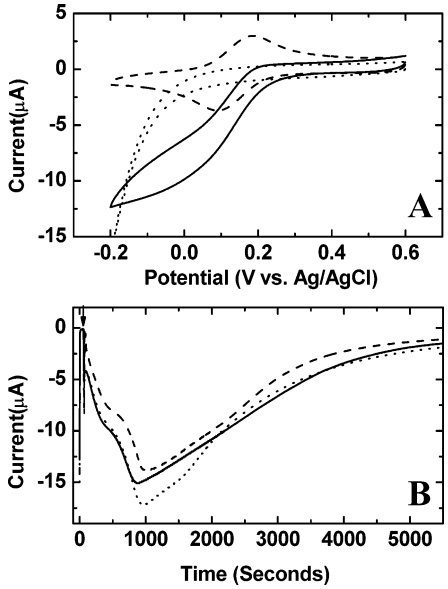

Figure 4. (A) Cyclic voltammograms of Au/Fe/PVP/GCE in 0.1 M acetate buffer in the absence (dashed line) and presence of 10 mM H_2O_2 (solid line). The dotted line was obtained from Au/PVP/GCE in the presence of 10 mM H_2O_2. The scan rate was 50 mV/s. (B) Time dependence of the cathodic current obtained at 0.1 V on Au/Fe/PVP/GCE rotated at 500 rpm in 0.1 M acetate buffer solution. 10 mM H_2O_2 was injected at time = 60 s (denoted by arrow). Au was deposited by three potential cycles between 0.8 and −0.2 V (solid), 10 potential cycles between 0.8 and −0.2 V (dashed), and a potential step from +0.8 to −0.2 V and holding at this potential for 60 s (dash−dot). The electrolyte solution was 1 mM $KAuCl_4$ + 0.1 M acetate buffer.

into and out of electroactive sites in the PVP film is inhibited after Au deposition. In separate experiments, we found that the peak currents increase linearly with the square root of the scan rate (data not shown). This linearity indicates that diffusion of electroactive species occurs within the polymer film and that semi-infinite diffusion conditions prevail at the fairly fast scan rates used here.[36]

Figure 3B shows the effect of time on the peak height observed for the $Fe^{III}(CN)_6^{3-}/Fe^{II}(CN)_6^{4-}$ couple in the Au/Fe/PVP/GCE system. After waiting for 30 min, the peak height and peak separation (135 mV initially, changing to 100 mV at 30 min) are nearly identical to the initial scan. The figure also shows the effect of electrode rotation on the $Fe^{III}(CN)_6^{3-}/Fe^{II}(CN)_6^{4-}$ couple. After 10 min rotation, the stationary voltammogram is identical to that obtained prior to rotation. These data show that the $Fe^{III}(CN)_6^{3-}/Fe^{II}(CN)_6^{4-}$ couple is substantially stabilized upon Au deposition relative to that found absent Au.

Figure 4A shows the cyclic voltammograms from the Au/Fe/PVP/GCE system in the presence (solid line) and absence (dashed line) of 10 mM H_2O_2 in 0.1 M acetate buffer, along with the Au/PVP/GCE system in 10 mM H_2O_2 + 0.1 M acetate buffer for comparison. The figure shows that, as was the case with the Fe/PVP/GCE system shown in Figure 2A, the catalytic reduction of H_2O_2 on begins around 0.15 V, which is after the cathodic peak potential of $Fe^{III}(CN)_6^{3-}/Fe^{II}(CN)_6^{4-}$ couple. However, the potential dependence of the reduction current with and without Au deposition is different. Absent Au, appreciable current associated with peroxide reduction appears at +0.10 V, while this current is in evidence as early as +0.25 V in the Au-deposited system. Additionally, the cathodic current increases with potential in the Au-decorated case. Absent $Fe(CN)_6^{3-}$, the system evinces no cathodic current at +0.10 V, which shows that Au alone is not sufficient for catalytic activity.

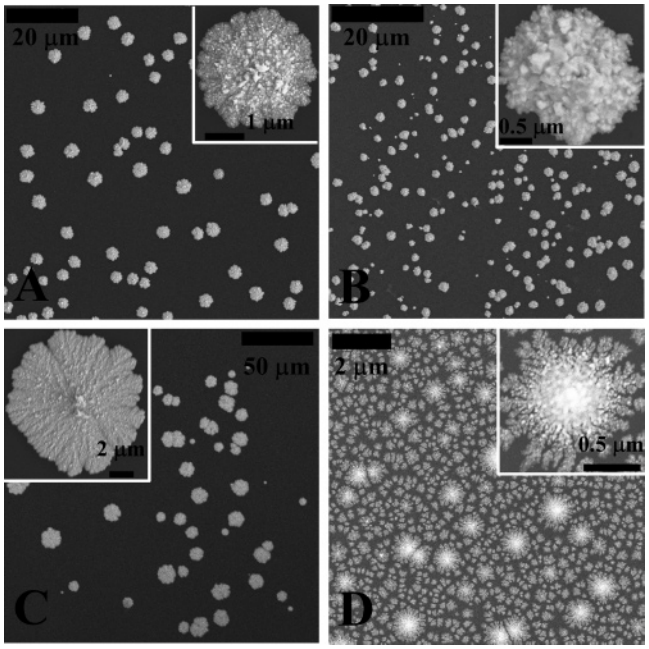

Figure 5. SEM images of Au particles deposited on PVP films in the presence (A−C) and absence (D) of $Fe(CN)_6^{3-}$ species in the films. The potential scheme for deposition was (A and D) three potential cycles between 0.8 and −0.2 V, (B) 10 potential cycles between 0.8 and −0.2 V, and (C) a potential step from +0.8 to −0.2 V and holding at this potential for 60 s. The electrolyte solution was 1 mM $KAuCl_4$ + 0.1 M acetate buffer.

TABLE 1: Particle Size and Surface Coverage

SEM image	average area (μm^2)	std dev (μm^2)	% coverage
A	10.7	2.6	7.24
B	2.8	2.1	11.7
C	47.2	30.6	7.21
D	0.041	0.078	41.0

Figure 4B shows the time-dependent current associated with peroxide reduction obtained from the Au/Fe/PVP/GCE system in 0.1 M acetate buffer following injection of sufficient peroxide to make $[H_2O_2] = 10$ mM. Three different Au preparations are shown, but all exhibit nearly the same behavior. The figure shows that the electroreduction current increases for a period of ca. 1000 s and then decreases exponentially with a time constant of ca. 5.2×10^{-4} s^{-1}. At ca. 6000 s, the current was only ca. 8% of its maximum value. The total amount of H_2O_2 consumed in the cell during this time period was less than 1% of the initial amount present.

3.3. Characterization of Au/Fe/PVP/GCE. To understand the origin of the stabilizing activity of the Au deposited on the Fe/PVP/GCE system, we characterized the system using microscopic and spectroscopic means.

3.3.1. SEM Imaging. Figure 5 shows SEM images obtained from the Au/Fe/PVP/GCE system following deposition of different amounts of Au. For comparison, the Au/PVP/GCE system is also shown. Table 1 gives average particle areas, standard deviations, and coverage for each system. Figure 5A shows the SEM image obtained following deposition of Au onto the Fe/PVP/GCE system by using three potential cycles between 0.8 and −0.2 V with a scan rate of 50 mV/s in a solution containing 1 mM $KAuCl_4$ + 0.1 M acetate buffer. The figure shows Au particles with an average diameter of ca. 3.7 μm distributed on the surface. The inset to Figure 5A shows one of these particles, which evinces a near circular shape albeit with some evidence for dendritic, tip-splitting behavior. The presence of nodules on the particle shows that this particle is not planar.

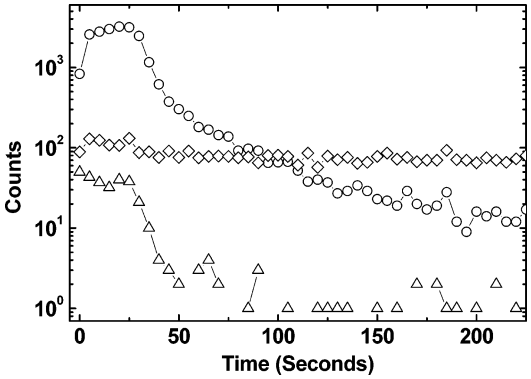

Figure 6. SIMS profile obtained from Au/Fe/PVP/GC electrode. Au was deposited by three potential cycles between 0.8 and −0.2 V in a solution containing 1 mM $KAuCl_4$ + 0.1 M acetate buffer. Secondary ion counts for Fe (○), C (◇), and Au (△) are plotted as a function of sputtering time.

Figure 5B shows the particles obtained following 10 cycles in the same solution used in Figure 5A. The image shows that the particles are somewhat smaller and more numerous on the PVP-coated GCE surface. While the size of the particles has decreased, the surface coverage has increased, as expected. The inset shows one of these particles.

Figure 5C shows particles obtained using the same solution as above, but deposited using a potential step from +0.8 to −0.2 V and holding at this potential for 60 s. The image shows that the particles are larger than those formed using the potential cycling methods, but that the surface coverage for this holding time is about the same as the three cycle deposition case shown in Figure 5A.

Finally, Figure 5D shows the particles obtained under the same conditions as reported for Figure 5A, with the absence of Fe incorporation into the PVP matrix. In contrast to the relatively sparse particle arrays reported in the presence of Fe incorporation, the Au deposits found here are considerably denser, evincing a surface coverage of over 40%. Additionally, the deposits feature the dendritic growth and tip-splitting behavior that is considered to be a hallmark of diffusion-limited aggregation. Deposits with this type of texture have been grown on other types of polymers.[37] The change in texture between the system absent Fe and those featuring Fe incorporation implies a strong role for Fe in the nucleation and growth of the Au deposit.

3.3.2. ToF SIMS. SIMS was employed to characterize the composition of Au/Fe/PVP films on GCE as a function of sputter depth. Figure 6 shows the SIMS profile obtained from an Au/Fe/PVP/GC electrode. The plot shows signals from Fe, Au, and C. The secondary ion counts from C are relatively constant across the time scale interrogated here, which is expected from a PVP film on a GCE surface. The secondary ion counts for Fe begin to decrease after 35 s of sputtering and reach background level after ca. 100 s. The secondary ion counts for Au show the same trends as those of Fe, in that they too fall off after 35 s and remain at background level after 100 s. The difference in the background level between Fe and Au can be explained in terms of the different SIMS relative sensitivity factors (RSFs) for these elements.[38] The RSF values are inversely proportional to the secondary ion counts for Fe and Au and are 2.4×10^{22} and 2.5×10^{24}, respectively.[39] Thus, the background counts for Fe will be at least an order of magnitude higher than the background counts for Au.

The same trends in secondary counts for Fe and Au indicate that these two elements have a similar distribution within the PVP film. SIMS data obtained from an Fe/PVP/GCE sample show the same trend for Fe distribution within the PVP film, which suggests that Au deposition does not strongly affect sites of Fe association within the film (data not shown).

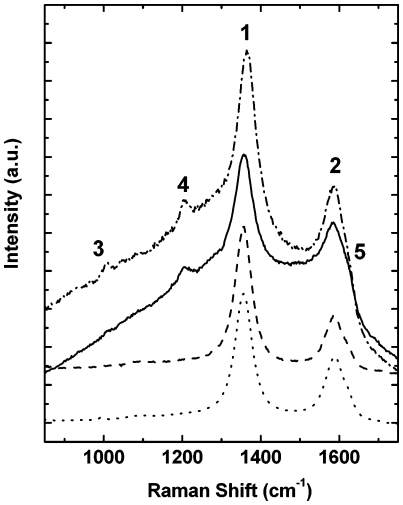

Figure 7. Raman spectra obtained from PVP/GCE (dotted), Fe/PVP/GCE (dashed), and Au/Fe/PVP/GCE (solid and dash−dot) films. Au was deposited by three potential cycles between 0.8 and −0.2 V in a solution containing 1 mM $KAuCl_4$ + 0.1 M acetate buffer. The excitation wavelength was 488 (dotted, dashed, and solid) and 458 nm (dash−dot).

3.3.3. Raman Spectroscopy. Figure 7 shows the results of ex situ Raman scattering measurements obtained from the PVP/GCE films considered in this paper. The dotted line in Figure 7 shows Raman scattering obtained with an excitation frequency of 488 nm from the PVP/GCE film. The spectrum evinces two intense peaks at 1357 and 1588 cm^{-1} (peaks 1 and 2, respectively), which are referred to as the D and G bands, respectively. The G band (peak 2) originates from an E_{2g} vibrational mode in single-crystalline graphite. The D band (peak 1) is observed in "unorganized" graphite materials such as pyrolytic graphite and glassy carbon and has been attributed an A_{1g} mode which becomes Raman active due to finite crystal size.[40,41]

Addition of $Fe(CN)_6^{3-}$ to the PVP film results in spectra (dashed line) that are nearly identical to those obtained absent the Fe complex between 200 and 2000 cm^{-1}. $Fe(CN)_6^{3-}$ ions adsorbed on metal surfaces exhibit several Raman bands in two spectral regions.[42−44] These regions are found between 300 and 600 cm^{-1} associated with Fe−C stretching modes and between 2100 and 2200 cm^{-1} associated with C≡N stretches.[42] We attempted to obtain Raman spectra from the Au/Fe/PVP/GCE system with an excitation wavelength of 680 nm, to utilize any putative surface enhanced Raman scattering (SERS) excitation available at this wavelength. However, no signal was observed. Interestingly, an earlier SERS study of PVP also reported the absence of signal from PVP on roughened Au.[45] At an excitation wavelength of 488 nm, the Raman spectroscopy (solid line in Figure 7) reveals two additional peaks at 1009 and 1206 cm^{-1}, (peaks 3 and 4, respectively) along with a shoulder at 1630 cm^{-1} (peak 5). Peak 3 is associated with a symmetric breathing mode, peak 4 is associated with a CH in-plane bending mode, and peak 5 is a ring CC stretch.[46] These peaks are somewhat more prominent with an excitation wavelength of 458 nm (dash−dot line in Figure 7). No other peaks were observed in the Raman spectrum.

4. Discussion

4.1. Origin of the Catalytic Activity of $Fe(CN)_6^{3-}$ Confined on Electrode Surfaces. Our results show that $Fe(CN)_6^{3-}$

activated by the PVP matrix exhibits catalytic activity for the electroreduction of H_2O_2. However, $Fe(CN)_6^{3-}$ species in solution is catalytically inactive. As mentioned in the Introduction, other Fe complexes such as Fe−porphyrin[11,12] and Fe-coordinated alizarin complexone[13] adsorbed on graphite electrode surfaces exhibit catalytic activity for H_2O_2 electroreduction. It should be noted that all of the Fe complexes studied in previous work exhibit an open coordination site on Fe. This open coordination site plays a role as a catalytically active site during the electroreduction of H_2O_2.[11,15] In the present work, the $Fe(CN)_6^{3-}$ species has no open coordination site on Fe, which might account for the absence of catalytic activity of $Fe(CN)_6^{3-}$ in solution phase. $Fe(CN)_6^{3-}$ is known to be very stable in solution phase, with an overall formation constant $\beta \sim 10^{44}$.[47] In particular, the equilibrium constant for replacement of one CN^- with H_2O for

$$Fe^{II}(CN)_6^{4-} + H_2O \rightleftarrows Fe(CN)_5H_2O^{3-} + CN^- \qquad (1)$$

is reported to range between $K = 8.3 \times 10^{-11}$ [48] and $K = 5 \times 10^{-9}$ [49] with similar numbers for the Fe^{III} species.

On the other hand, $Fe(CN)_6^{3-}$ species confined on the electrode surface shows catalytic activity as described above. Thus, $Fe(CN)_6^{3-}$ species should have open coordination sites when they are confined on the electrode surface. In the presence of pyridine (Py), the CN^- ligand becomes more labile. For example, for

$$Fe^{III}(CN)_6^{3-} + Py \rightleftarrows Fe(CN)_5Py^{2-} + CN^- \qquad (2)$$

the equilibrium constant can be determined to be $K = 1.3 \times 10^{-5}$,[48] which is at least some 4 orders of magnitude greater than that found for CN^- replacement by water. This result suggests that the $Fe(CN)_6^{3-/4-}$ center becomes more labile in the presence of Py, a result that is consistent with our observation of catalytic activity from Py-stabilized $Fe(CN)_6^{3-}$. Additionally, the ca. 40 mV cathodic shift of the E_{mid} upon incorporation into the PVP matrix is consistent with an Fe center where an anionic CN^- ligand is replaced by neutral Py, although other effects, such as the environmental change between solution and surface, could also contribute to this shift.

4.2 Stabilization of Catalytic Activity with Au Deposition. An important observation arising from this work is that deposition of Au onto the PVP/Fe/GCE system results in an order-of-magnitude stabilization of the H_2O_2 electroreduction response as shown by comparing Figures 2B and 4B. The origin of this stabilization is prevention of leaching of the Fe center in the presence of the Au deposit. Interestingly, differences in Au deposition conditions do not result in substantial changes in the time dependence of the response of the system toward H_2O_2 reduction. All of the cases examined here exhibited a period where catalytic activity increases, followed by a nearly exponential decay. This response does not depend on the amount (Figure 5B) or the particle size (Figure 5C) of deposited Au particles. A period of increasing reduction current is also seen for the Fe/PVP/GCE system before Au deposition. The increase in reduction current presumably originates in the increased access of Fe sites to the peroxide reactant, resulting either from percolation or from the aforementioned liability of the Fe−Py bond. In the absence of leaching, these effects could in principle be distinguished by fitting the temporal response to a model. However, the presence of leaching makes this fit complicated and therefore was not attempted here. The plateau region in Figure 2B might be the result of increase of catalytic activity as well as the loss of $Fe(CN)_6^{3-}$ species due to electrode rotation.

The insensitivity of the time dependence of the catalytic response to Au deposition conditions suggests that initial stages of Au deposition are most important. In particular, the stability arises from nucleation of Au species in and on top of the film that is not enhanced by subsequent growth. Our observation using SIMS that Au is distributed throughout the polymer film in the same manner as Fe suggests that this initial nucleation does indeed occur at sites both within and on top of the film.

The presence of Au evenly distributed throughout the PVP film suggests that the Fe center is coordinated or tethered to Au nuclei, which then retard the solubility of the Fe. One possibility is formation of an Fe−CN−Au bridge analogous to that found in Prussian Blue type compounds.[50] It is known that CN ligands are able to provide linkages between Fe and other metal atoms such as Ru, Co, Ni, and Cu.[51,52] In particular, cyano-bridged compounds containing an M−CN−Au−CN−M type linkage has been reported in previous work.[53] Unfortunately, we were not able to observe bands in the C−N stretch region or the low energy M−ligand stretch region which could place our contention on a firmer basis.

4.3. Au Deposition Behavior. As deposition proceeds, most of the growth occurs at sites that are easily accessible to solution Au species, that is, the surface. We show that we can control the amount of Au on the surface and the size of the Au clusters by changing deposition conditions. However, these growing clusters do not change the catalytic response of the system.

That the presence of Fe changes the location of the initial nucleation is dramatically shown by comparing Figure 5A−C with Figure 5D. In the absence of Fe centers within the film, Au nucleation occurs more or less uniformly on the PVP surface, because subsequent images such as that in Figure 5D show evenly distributed particles. A similar result was reported for Au deposition onto a polystyrenesulfonate/polydiallylamino-ethylammonium multilayer.[37] On thin films of polypyrrole, Au deposition is thought to occur via a process involving three-dimensional instantaneous nucleation, but as the film becomes thicker, three-dimensional progressive nucleation becomes dominant.[54] For the thick films used here, the tip-splitting behavior observed is consistent with this latter mechanism.

Alternatively, the presence of Fe centers within the film provides additional locations for Au particle nucleation and, as a result, nucleation occurs within as well as on top of the film. This change in location of initial nucleation strongly changes the morphology of Au particles in subsequent growth. The Fe centers might enhance electron transfer at the interface, or provide current paths through the PVP film which would serve to disperse nucleation sites.

5. Conclusions

We showed that $Fe(CN)_6^{3-}$ can function as a catalyst for the electroreduction of H_2O_2 on a PVP-modified glassy carbon electrode. In solution, $Fe(CN)_6^{3-}$ is not labile and exhibits no open coordination sites that can be used for peroxide coordination. Upon incorporation into the PVP film, however, the presence of Py functionality in the film increases the lability of the Fe center, resulting in catalytic activity.

We also showed that leaching of the Fe complex from the PVP film is the major route to catalyst inactivation. An order of magnitude increase in stability of the catalyst could be obtained by decoration of the Fe/PVP/GC surface with electrodeposited Au. The Au presumably coordinates to the Fe center via bridging CN groups. The presence of Fe changes the Au deposit morphology, by providing nucleation sites for Au both within and atop the film.

The results provided in this paper show that a simple catalytic system can be stabilized through Au nanoparticle deposition. Future work will concentrate on the design of appropriate bridging ligands to achieve even greater stabilization.

Acknowledgment. J.K. thanks the Department of Chemistry for financial support in the form of a Walter Burrows Brown Fellowship in Chemical Research. SEM and ToF SIMS measurements were carried out in the Center for Microanalysis of Materials, University of Illinois, which is partially supported by the U.S. Department of Energy under Grant DEFG02-91-ER45439. Raman measurement was carried out in the Laser and Spectroscopy Facility of the Frederick Seitz Materials Research Laboratory, University of Illinois, which is partially supported by the U.S. Department of Energy under Grant DEFG02-91-ER45439. This work was funded by the NSF (CHE-0237683), which is gratefully acknowledged.

References and Notes

(1) Tarasevich, M. R.; Sadkowski, A.; Yeager, E. In *Comprehensive Treatise of Electrochemistry*; Conway, B. E., Bockris, J. O. M., Yeager, E., Kahn, S. U. M., White, R. E., Eds.; Plenum: New York, 1983; Vol. 7, pp 301−398.

(2) Adzic, R. R. In *Electrocatalysis*; Lipkowski, J., Ross, P. N., Eds.; Wiley-VCH: New York, 1998; pp 197−242.

(3) Mukerjee, S.; Srinivasan, S.; Soriaga, M. P.; McBreen, J. *J. Phys. Chem.* **1995**, *99*, 4577−4589.

(4) Schmidt, T. J.; Stamenkovic, V.; Arenz, M.; Markovic, N. M.; Ross, P. N. *Electrochim. Acta* **2002**, *47*, 3765−3776.

(5) Zhang, J.; Mo, Y.; Vukmirovic, M. B.; Klie, R.; Sasaki, K.; Adzic, R. R. *J. Phys. Chem. B* **2004**, *108*, 10955−10964.

(6) Solomon, E. I.; Sundaram, U. M.; Machonkin, T. E. *Chem. Rev.* **1996**, *96*, 2563−2605.

(7) Mano, N.; Fernandez, J. L.; Kim, Y.; Shin, W.; Bard, A. J.; Heller, A. *J. Am. Chem. Soc.* **2003**, *125*, 15290−15291.

(8) Soukharev, V.; Mano, N.; Heller, A. *J. Am. Chem. Soc.* **2004**, *126*, 8368−8369.

(9) Fernandez, J. L.; Walsh, D. A.; Bard, A. J. *J. Am. Chem. Soc.* **2005**, *127*, 357−365.

(10) Collman, J. P.; Marrocco, M.; Denisevich, P.; Koval, C.; Anson, F. C. *J. Electroanal. Chem.* **1979**, *101*, 117−122.

(11) Shigehara, K.; Anson, F. C. *J. Phys. Chem.* **1982**, *86*, 2776−2783.

(12) Jiang, R. Z.; Dong, S. J. *Electrochim. Acta* **1990**, *35*, 1227−1232.

(13) Zhang, J. J.; Anson, F. C. *J. Electroanal. Chem.* **1993**, *353*, 265−280.

(14) Zhao, C. P.; Galazka, M.; Cheng, I. F. *J. Electroanal. Chem.* **1994**, *379*, 501−503.

(15) Toth, J. E.; Melton, J. D.; Cabelli, D.; Bielski, B. H. J.; Anson, F. C. *Inorg. Chem.* **1990**, *29*, 1952−1957.

(16) Mizuno, N.; Nozaki, C.; Kiyoto, I.; Misono, M. *J. Am. Chem. Soc.* **1998**, *120*, 9267−9272.

(17) Mizuno, N.; Nozaki, C.; Kiyoto, I.; Misono, M. *J. Catal.* **1999**, *182*, 285−288.

(18) Oyama, N.; Anson, F. C. *J. Am. Chem. Soc.* **1979**, *101*, 739−741.

(19) Oyama, N.; Anson, F. C. *J. Am. Chem. Soc.* **1979**, *101*, 3450−3456.

(20) Oyama, N.; Anson, F. C. *Anal. Chem.* **1980**, *52*, 1192−1198.

(21) Oyama, N.; Anson, F. C. *J. Electrochem. Soc.* **1980**, *127*, 249−250.

(22) Oyama, N.; Anson, F. C. *J. Electrochem. Soc.* **1980**, *127*, 640−647.

(23) Shimomura, T.; Oyama, N.; Anson, F. C. *J. Electroanal. Chem.* **1980**, *112*, 265−270.

(24) Zumbrunnen, H. R.; Anson, F. C. *J. Electroanal. Chem.* **1983**, *152*, 111−124.

(25) Shiu, K. K.; Anson, F. C. *J. Electroanal. Chem.* **1991**, *309*, 115−129.

(26) Kao, W. H.; Kuwana, T. *J. Am. Chem. Soc.* **1984**, *106*, 473−476.

(27) Kost, K. M.; Bartak, D. E.; Kazee, B.; Kuwana, T. *Anal. Chem.* **1990**, *62*, 151−157.

(28) Bartak, D. E.; Kazee, B.; Shimazu, K.; Kuwana, T. *Anal. Chem.* **1986**, *58*, 2756−2761.

(29) Li, Y. J.; Lenigk, R.; Wu, X. Z.; Gruendig, B.; Dong, S. J.; Renneberg, R. *Electroanalysis* **1998**, *10*, 671−676.

(30) Coutanceau, C.; Croissant, M. J.; Napporn, T.; Lamy, C. *Electrochim. Acta* **2000**, *46*, 579−588.

(31) Shan, J. N.; Pickup, P. G. *Electrochim. Acta* **2000**, *46*, 119−125.

(32) Keita, B.; Nadjo, L.; Haeussler, J. P. *J. Electroanal. Chem.* **1988**, *243*, 481−491.

(33) Bard, A. J.; Faulkner, L. R. *Electrochemical Methods*, 2nd ed.; John Wiley & Sons: New York, 2001.

(34) Lindholm, B.; Sharp, M. *J. Electroanal. Chem.* **1986**, *198*, 37−52.

(35) Peerce, P. J.; Bard, A. J. *J. Electroanal. Chem.* **1980**, *114*, 89−115.

(36) Martin, C. R.; Rubinstein, I.; Bard, A. J. *J. Am. Chem. Soc.* **1982**, *104*, 4817−4824.

(37) Zhang, X.; Shi, F.; Yu, X.; Liu, H.; Fu, Y.; Wang, Z. Q.; Jiang, L.; Li, X. Y. *J. Am. Chem. Soc.* **2004**, *126*, 3064−3065.

(38) Wilson, R. G.; Stevie, F. A.; Magee, C. W. *Secondary Ion Mass Spectroscopy*; John Wiley & Sons: New York, 1989.

(39) Wilson, R. G. *Int. J. Mass Spectrom. Ion Processes* **1995**, *143*, 43−49.

(40) Tuinstra, F.; Koenig, J. L. *J. Chem. Phys.* **1970**, *53*, 1126−1130.

(41) Kawashima, Y.; Katagiri, G. *Phys. Rev. B* **1995**, *52*, 10053−10059.

(42) Fleischmann, M.; Graves, P. R.; Robinson, J. *J. Electroanal. Chem.* **1985**, *182*, 87−98.

(43) Loo, B. H. *Chem. Phys. Lett.* **1993**, *213*, 479−484.

(44) Loo, B. H.; Lee, Y. G.; Liang, E. J.; Kiefer, W. *Chem. Phys. Lett.* **1998**, *297*, 83−89.

(45) Garrell, R. L.; Beer, K. D. *Langmuir* **1989**, *5*, 452−458.

(46) Roth, P. G.; Boerio, F. J. *J. Polym. Sci., Part B: Polym. Phys.* **1987**, *25*, 1923−1933.

(47) Perera, W. N.; Hefter, G. *Inorg. Chem.* **2003**, *42*, 5917−5923.

(48) James, A. D.; Murray, R. S. *J. Chem. Soc., Dalton Trans.* **1975**, 1530−1533.

(49) Beck, M. T. *Pure Appl. Chem.* **1987**, *59*, 1703−1720.

(50) Vahrenkamp, H.; Geiss, A.; Richardson, G. N. *J. Chem. Soc., Dalton Trans.* **1997**, 3643−3651.

(51) Richardson, G. N.; Vahrenkamp, H. *J. Organomet. Chem.* **2000**, *594*, 44−48.

(52) Sheng, T. L.; Appelt, R.; Comte, V.; Vahrenkamp, H. *Eur. J. Inorg. Chem.* **2003**, 3731−3737.

(53) Deeming, A. J.; Proud, G. P.; Dawes, H. M.; Hursthouse, M. B. *Polyhedron* **1988**, *7*, 651−657.

(54) Hwang, B. J.; Santhanam, R.; Lin, Y. L. *Electroanalysis* **2003**, *15*, 1667−1676.